Received: 17 April 2021 | Revised: 28 July 2021 | Accepted: 29 July 2021

DOI: 10.1002/jrs.6234

RESEARCH ARTICLE

Journal of RAMAN SPECTROSCOPY WILEY

Cathodoluminescence, Raman and scanning electron microscopy with energy dispersion system mapping to unravel the mineralogy and texture of an altered Ca—Al-rich inclusion in Renazzo CR2 carbonaceous chondrite

Mario Tribaudino[1] | **Danilo Bersani**[2] | **Luciana Mantovani**[1] | **Mattia Pizzati**[1] | **Giancarlo Salviati**[3]

[1]Department of Chemical, Life and Environmental Sustainability Sciences, University of Parma, Parma, Italy

[2]Department of Mathematical, Physical and Computer Sciences, University of Parma, Parma, Italy

[3]Institute of Materials for Electronics and Magnetism (IMEM-CNR), Parma, Italy

Correspondence
Mario Tribaudino, Department of Chemical, Life and Environmental Sustainability Sciences, University of Parma, Parco Area delle Scienze 157/a, Parma 43124, Italy.
Email: mario.tribaudino@unipr.it

Present address
Mario Tribaudino, Department of Earth Sciences, University of Torino, Torino, Italy

Funding information
'Departments of Excellednce' program of the Italian Ministry for Education, University and Research

Abstract

An altered fluffy type A Ca—Al-rich inclusion in the CR2 Renazzo carbonaceous chondrite was examined by combined Raman, scanning electron microscopy with energy dispersion system (SEM-EDS) and cathodoluminescence (CL) mapping. Blue CL at 450 nm and orange emission at 600 nm were related to anorthite and calcite, respectively. Raman spectra were highly fluorescent, and only the stronger peaks of anorthite, clinopyroxene and calcite were observed. Raman-induced fluorescence emission was measured using the 632-nm Raman laser source, up to 850 nm, and used to chart the mineral phases. A fluorescence structured peak at 690 nm, split in three subpeaks at 678, 689 and 693 nm, was found; it is likely related to the fluorescence emission of Cr^{3+} from a fassaitic pyroxene in anorthite. Secondary pyroxene in the Wark–Lovering rim does not show the peak at 690 nm; the different fluorescence emission from the secondary rim and the pyroxene patches within anorthite could be a marker to spot the primary pyroxene. From combined imaging, the events in the altered chondrite could be sequenced. Starting from a pristine assemblage of spinel and melilite, with little fassaite, several alteration episodes occurred. Alteration in secondary anorthite, which could be mapped by the blue CL emission at 450 nm, was followed by alkalization, with rims of sodalite and nepheline, and subsequent formation of secondary clinopyroxene, encircling the inclusion. Widespread calcite alteration, present also in the matrix between chondrules, was the last recorded event.

KEYWORDS

Ca—Al-rich inclusions, cathodoluminescence, photoluminescence, Raman mapping, SEM-EDS

1 | INTRODUCTION

Ca—Al-rich inclusions (CAIs) are among the most pristine objects in the Solar System. They are formed by early condensation of alkali- and volatile-free refractory phases, in a highly reducing environment.[1] CAIs are found in carbonaceous chondrites and appear as inclusions from millimetre to micrometre sized, grey-whitish in colour, irregularly shaped and often ameboidal-fluffy structured.[1,2] Their age of 4567.3(2) My[3] possibly slightly predates the formation of chondrules and thus can mark the very beginning of the condensation of the Solar System.[4] Primary mineral components are anorthite, pyroxene, spinel, melilite, grossite, hibonite and perovskite; secondary reactions introduced alkali-bearing phases like nepheline and/or sodalite, as well as other phases like andradite, hedenbergite and secondary anorthite.[1] In several issues, their composite structure, the tiny size of the crystals, often barely resolvable at optical observation, or less, and the widespread alteration makes the analysis of CAI a daunting task. To unravel the relations between the forming minerals, combined use of several analytical techniques is fruitful. Chemical differences can be enhanced by scanning electron microscopy with energy dispersion system (SEM-EDS) mapping, which is composition sensitive, together with spectroscopic techniques, which are phase sensitive, among which Raman spectroscopy. Raman peaks identify given phases, and their mapping charts the phase distribution at the micron scale. An advantage is that phases with similar composition, which may overlap in a SEM-EDS mapping, are detected by their distinctive Raman signature. However, Raman spectroscopy is often biased by the defective nature of minerals in meteorites, which experienced long-term exposition to cosmic radiation and were shocked at several points of their history. This results in a fluorescence that conceals the Raman signal. Laser-induced fluorescence (photoluminescence [PL]) is usually treated as noise when collecting Raman spectra, but it can bear interesting compositional information. Fluorescence micromapping obtained with Raman apparatus has the potential to show, in a single Raman experiment, the emitting elements that are present as impurities or within inclusions in a phase identified by a specific Raman spectrum. Moreover, also when the fluorescence cannot be easily ascribed to a specific element, it may show spectral features that may identify the fluorescent phase. The highly fluorescent nature of the phases composing the CAIs provides an opportunity for a combined investigation using both Raman peaks and fluorescence emission from the same point. Such analysis on CAIs is expected to show in detail the distribution of the emitting ions in the different phases.

PL and SEM cathodoluminescence (SEM-CL) in the study of meteorites have been also used (e.g., Hutcheon et al. and Akridge et al.[5,6]): the highly defective nature of minerals in shocked meteorites promotes the presence of several CL centres, which can be related to the crystallization, environmental and shock history. More rarely CL has been used in the analysis of CAI (e.g., Garcia-Guinea et al.[7]). CL and PL, the latter either as a by-product of a Raman or in devoted experiment, can be considered complementary techniques. CL emission is a radiation, typically in the UV–VIS–NIR region, induced by an electron beam interacting with crystal defects or colour centres, usually obtained in an electron microscope. Also, PL occurs from an interaction with defects and transition elements. The analysed signal is in both cases a luminescence emission, but the efficiency of different emission centres is very different moving from SEM-CL to PL. In addition, the two techniques have peculiar advantages and drawbacks that allow to integrate and widen the range of obtained information. The main advantage of PL is the excellent spectral resolution; the main drawback compared with SEM-CL is the lower injection power and spatial resolution both in spectroscopy and imaging modes. The main advantages of SEM-CL with respect to PL are the higher in-depth and lateral resolution, the continuously on-line variable injection power as well as the concurrent use of spectral and mapping EDS. The main disadvantage of CL is the lower spectral resolution, due to the hot carrier thermalization, which results in larger full width at half maximum (FWHM) spectra.

Here, we investigate an altered fluffy CAI in the carbonaceous CR2 Renazzo chondrite. In this holotypic chondrite, we have found a highly altered inclusion, in which the primary texture was subject of alkaline alteration, followed by subsequent carbonation. The sequence of alterations resulted in a wealth of minerals within the grains, whose texture is hardly constrained. Highly fluorescent Raman spectra were observed: the fluorescence, which is generally considered a nuisance in the interpretation of Raman spectra, was here used in connection with the Raman emission to map the mineral phases and their reactions. The inclusion in Renazzo CR2 is especially challenging, as highly altered, and with a complex mineral texture. It proves particularly suitable to test the combined information from Raman emission and laser-induced fluorescence in the same experiment, in comparison with other techniques like SEM-EDS mapping and CL. To our knowledge, Raman fluorescence was used here for the first time in meteoritic research.

The combination with emissions induced by CL, SEM-EDS imaging and chemical mapping constrained the mineral texture of the inclusion, giving a picture of

the stages of formation, to unravel the phase relations within the CAI and detail the onset of the alteration during the condensation of the inclusion.

2 | MATERIALS AND METHODS

2.1 | Sample

The Renazzo CR2 meteorite is a historical meteorite, fallen on 15 January 1824. A sample weighing 11 g from the original 10 kg[8] is stored in the Mineralogical Museum of the University of Parma. It appears as a black rock with visible chondrules.

A thin section was made from the original sample and glued in epoxid for fixing and avoiding de-gassing during SEM-EDS analysis. Then, it was thinned and exposed in air. The glue is about 30 microns below the surface, and it was never reached by laser or electron beam (Figures 1 and 2).

The sample was observed by Raman and optical CL without coating, then carbon coated for SEM-EDS and eventually gold coated for SEM-CL.

2.2 | Optical CL

Optical CL was performed in several selected areas of the thin section. Images were acquired with a CITL CL Mk5-2 cold CL apparatus (beam current of 250 μA and 10 kV and operating vacuum of 0.035 mbar), coupled with a Leica DM 7200M standard petrographic microscope. The microscope was equipped with a Leica DFC 450C high sensitivity camera, suitable to operate on low-luminescence samples. All images were acquired at 5 × magnification, with an image resolution of 3840 × 2880 pixels, having care to maintain the exposure time between 7 and 8 s.

An image of the Ca-Al inclusion is shown in Figure 3.

2.3 | SEM-CL

SEM-CL spectroscopy and imaging have been performed in a S360 Cambridge SEM equipped with a GatanMonoCL system (1800 lines/mm grating, multialkali photomultiplier sensitive in the range 350–830 nm). The spectra have been collected at an accelerating voltage of 10 kV, a beam current of 10 nA and a spectral resolution of 9 nm. The data were collected at room temperature both in imaging and spectroscopy setting. Data collection lasted on the average a few minutes in spectroscopy mode, 15–20 s in panchromatic imaging and 60–80 s in monochromatic imaging. To avoid charging effects, the sample was beforehand covered with a 100-nm-thick gold layer.

Only the section containing the CAI was investigated due to the size of the sample spectrometer. A sample spectrum and the CL image of the area from which it was taken is shown in Figure 4.

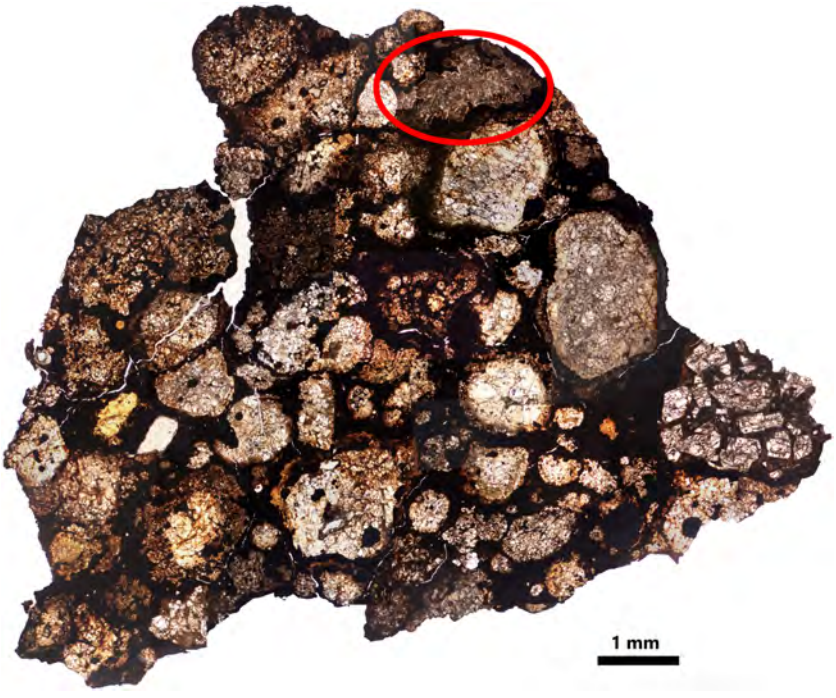

FIGURE 1 Thin section (parallel polars) of the Renazzo CR2 chondrite. The red ellipse shows the location of the Ca—Al-rich inclusion [Colour figure can be viewed at wileyonlinelibrary.com]

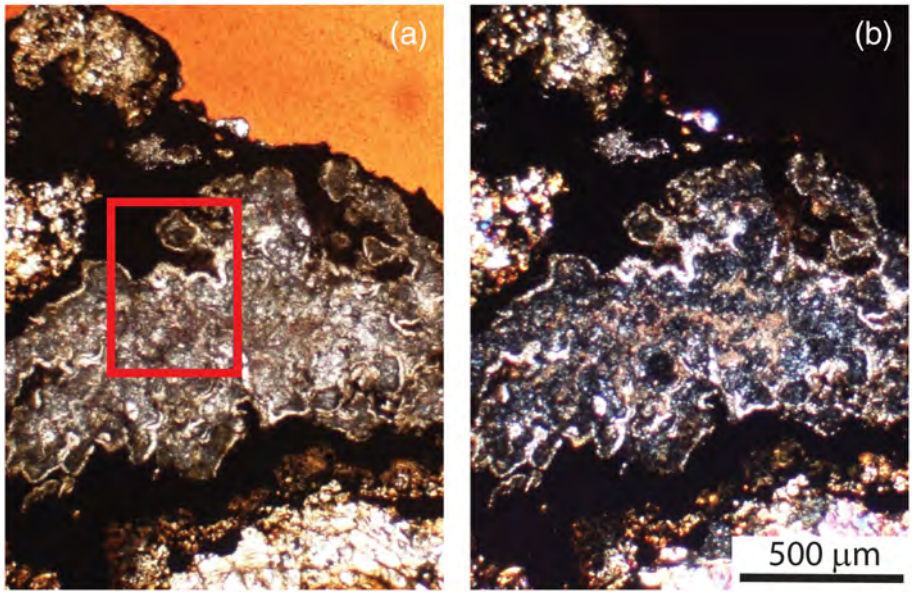

FIGURE 2 Transmitted light microscopic images with sample in-between (a) parallel and (b) crossed polarizers. The red rectangle indicates the area of the scanning electron microscopy with energy dispersion system (SEM-EDS) mapping in Figure 5 [Colour figure can be viewed at wileyonlinelibrary.com]

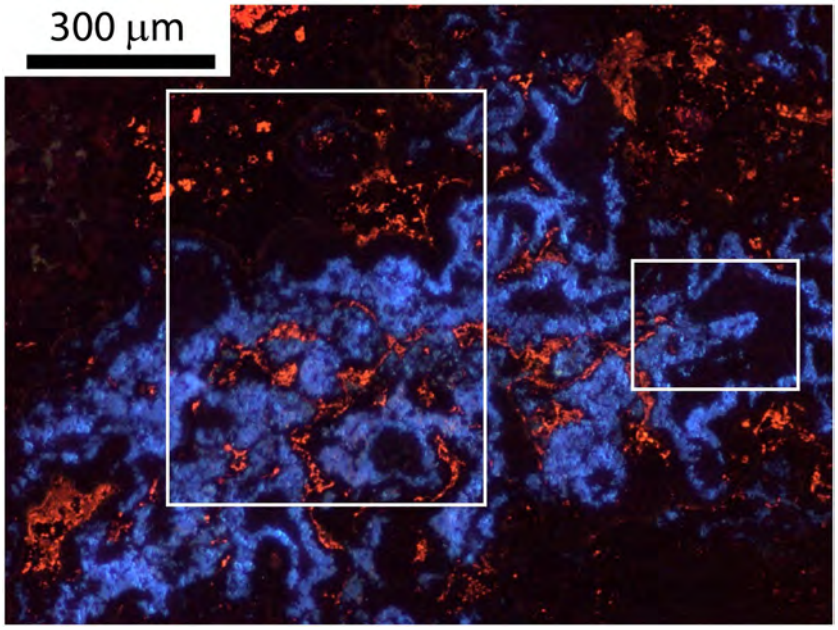

FIGURE 3 Optical cathodoluminescence image of the Ca—Al-rich inclusion. Emissions from calcite, orange; anorthite, blue. The left inset refers to the area imaged in Figure 5, the right one to that imaged in Figure 4 [Colour figure can be viewed at wileyonlinelibrary.com]

2.4 | Scanning electron microscopy with energy dispersion system

The CAI and the surrounding matrix were examined by SEM-EDS, using a Jeol 6400 SEM, equipped with an Oxford-INCA EDS, operated at 15 kV. Spot analyses in the whole inclusion and a compositional map were taken. The map was done in an area of 480 × 610 µm^2, part of which was further investigated by Raman and fluorescence emission mapping, at a resolution 256 dpi, during repeated scanning for 3 h and dwell time of 100 µs/pixel (Figure 5). The size of the analytical spot is about 1–2 µm. The analytical values from the map were used to identify the phases and obtain their mineralogical composition. This was done using AZTEC 3.3 software (Oxford instruments).

Compositional maps for the investigated elements are reported as Figure S1.

2.5 | Raman mapping

Raman spectra were taken all over the inclusion, whereas Raman mapping was done in the area shown in Figure 5. A Horiba LabRam with 1800 lines/mm grating and a charge-coupled device (CCD) detector with an array of

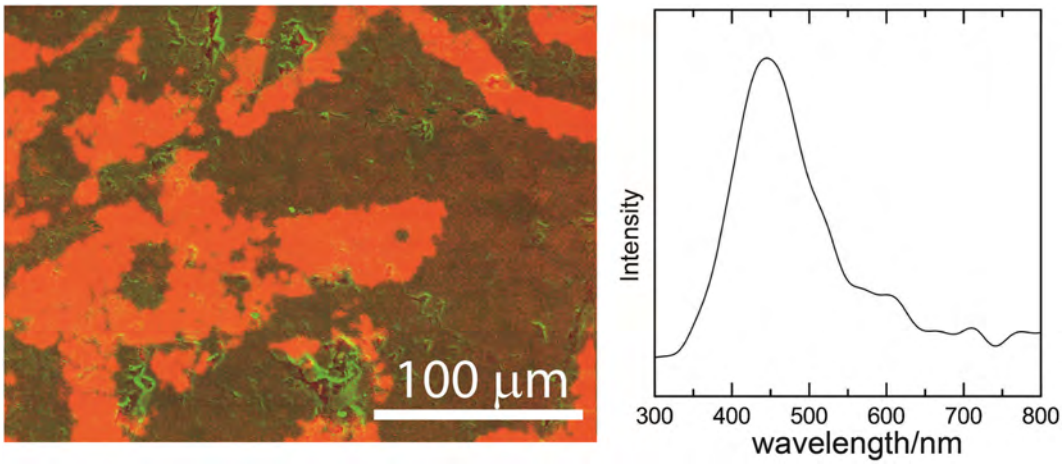

FIGURE 4 Scanning electron microscopy cathodoluminescence (SEM-CL) image, left, and relevant emission spectrum (right). The emission is only from anorthite (orange false colour). The green/dark green features are due to surface morphology and are specimen areas with no CL emission [Colour figure can be viewed at wileyonlinelibrary.com]

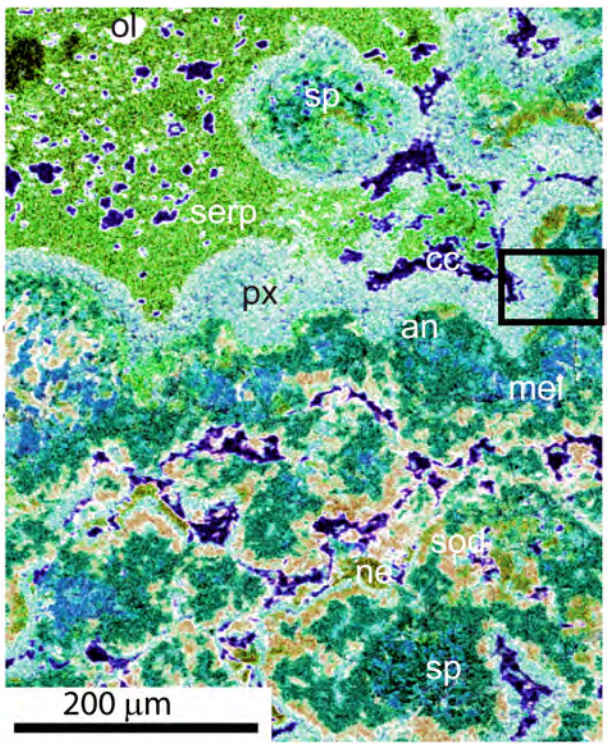

FIGURE 5 Energy dispersion system (EDS) map from superimposed Na, Mg, Si, Ca and Al maps. Element maps are in Figure S1. Dark blue: calcite, cc; light green: Fe—Mg serpentine, serp; dark green: anorthite, an; blue: melilite, mel; brown: sodalite, sod; light blue-green fassaite pyroxene, px, with whitish rim of diopside; white (external to Ca—Al-rich inclusion [CAI]) olivine, ol; black and blue: spinel, sp; brown-green: nepheline, ne. The black rectangle indicates the area of the Figure 8 [Colour figure can be viewed at wileyonlinelibrary.com]

1,024 × 256 pixels was used. The excitation was obtained with the 632.8-nm line of a He—Ne laser and the 473-nm line of a doubled Nd:YAG laser. A filter wheel was used to reduce the laser power on the sample to 1 mW or less on the sample. The wavenumber calibration was performed against the Raman peak of silicon. A 100× objective with a 0.9 numerical aperture and a 150-µm confocal hole were used. Spatial resolution was about 1 µm, and the spectral resolution was 2 cm^{-1} with an accuracy of 0.5 cm^{-1}. Collection time of the spectra ranged from 3 to 12 min (typical exposures were 60–240 s, repeated 3 times), depending upon the crystal size, the Raman scattering efficiency, and the intensity of the background fluorescence. Laser-induced fluorescence was always present.

In the small area shown in Figure 5, Raman mapping was done, with the 632-nm laser source. The area, sized 80 × 48 μm^2, was sampled at a step of 4 µm along both x and y axes. A first scan was done on the lower wavenumber range, from 50 to 1105 cm^{-1}, focused on the analysis of the Raman peaks; a second scan was then done in an extended range, from 100 to 4000 cm^{-1} (up to 900 nm), for the study of fluorescence.

3 | RESULTS AND DISCUSSION

3.1 | Optical microscopy

Thin section observation showed chondrules of porphyric olivine (PO), porphyric olivine–pyroxene (POP) and

radial pyroxene (RP), within a matrix of Fe—Mg silicate oxides and hydroxides. Alteration of chondrules at the boundaries in serpentine and smectite is apparent, as previously reported.[9,10] In the thin section, an elongated, curly feature was observed (Figure 1), identified as a CAI; it will be the focus of the present investigation.

Optical microscopy on the CAI shows a Wark–Lovering ring of pyroxene,[1] which envelopes the entire inclusion. Wark–Lovering rings are concentric monomineralic rings, related to different condensation phases.[11] In the inclusion, a fine mineral aggregate is present, non-recognizable by optical microscopy alone. Few grains, octahedral shaped and a high birefringent phase, subsequently identified as spinel and calcite, respectively, coexist in a low birefringent polycrystalline matrix (Figure 2).

3.2 | SEM-EDS analyses

The map in Figure 5 shows a structure made by concentric rims with a core of altered spinel and melilite grains. They are patchily distributed, in a matrix with secondary anorthite prevailing. The assemblage of spinel, anorthite and melilite is enveloped by alkaline minerals, nepheline and sodalite, and, on an outer rim, by fassaitic clinopyroxene. A larger fassaitic rim encircles the inclusion, with composition closer to diopside at the outer border. An irregular layer of calcite further encircles the fassaite; calcite is also present outside the inclusion. In the chondrite matrix, we find an assemblage of serpentine, Fe—Ni kamacite and Mg-rich olivine. The contact between anorthite and melilite is blurred, suggesting a pervasive and inhomogeneous reaction. Some fassaitic pyroxene was found within the CAI, unrelated with the above pyroxene rims. It appears in patches few micrometres sized, together with anorthite. The suggestion is that it is a primary phase. Anorthite, as shown in subsequent optical CL analysis, is convoluted and encircles spinel and melilite. We may then assume that anorthite is mostly secondary, formed in reaction with melilite, and that spinel and melilite with minor fassaite were the primary minerals. The primary assemblage, together with the shape of the inclusion, provides evidence to classify the CAI as a fluffy A type CAI.

The chemical composition of the pyroxene changes from almost pure diopside in the outer part of the Wark—Lovering rim (white in Figure 5) to that of a typical fassaite (light green). The composition of the average rim fassaite is $Ca_{1.00}(Al_{0.15}Mg_{0.72}Ti_{0.06}Fe_{0.05}Cr_{0.02})(Al_{0.15}Si_{1.85})O_6$. The pyroxene in patches with anorthite has a higher Al content than rim pyroxene, with average composition $Ca_{1.01}(Mg_{0.35}Ti_{0.14}Al_{0.34})(Al_{0.46}Si_{1.54})O_6$. Anorthite analyses show Mg between 0.16 and 1.58 wt%, Fe up to 1.85 wt% and eventually a variable Cr content, between 0.05 and 0.45 Cr wt%. This relatively high value for Cr, to our knowledge, was not previously observed in feldspars: in the early compilation by Smith and Brown,[12] Cr does not exceed 100 ppm. We suggest that Cr comes from some inclusion in the plagioclase, which however was not identified by subsequent Raman analysis. Due to the size of the analytical spot, it is likely the presence of submicrometric sized inclusions of a Cr richer phase. Neglecting Fe, Mg and Cr the plagioclase is almost completely anorthitic ($Ca_{0.99}Na_{0.01}Al_{1.98}Si_{2.01}O_8$). Melilite composition on average is $Ca_{1.95}Na_{0.05}(Mg_{0.18}Al_{1.59}Si_{1.23})O_7$, that is, $Geh_{77}Ak_{18}Na\text{-}Ak_5$. The spinel is almost pure spinel with little Fe content, $Mg_{0.89}Fe_{0.12}Al_{1.99}O_4$. Sodalite crystal chemical composition is $(Na_{4.34}Ca_{0.15}Mg_{0.49}K_{0.05})(Si_{6.24}Al_{5.54}Fe_{0.37})Cl_2O_{24}$. In this formula, we have a charge equilibrium, at the expense of a significant deviation from the stoichiometry, which expects close to 8 atoms of Na per formula unit. Such result would require significant loss of Na.

In no point Ti-rich oxides like hibonite or perovskite are found.

3.3 | Cathodoluminescence

CL spectroscopy showed two emissions, one orange, in the matrix and the inclusion, the other blue in the inclusion. The orange emission is interstitial, whereas the blue one appears as a convoluted ribbon in the inclusion, bordering the external rim of clinopyroxene (Figure 1). SEM-EDS analyses on the same areas showed that the orange emission comes from calcite, whereas the blue one from anorthite. Shades of lighter or darker colour were observed, but we did not find evidence that the emission comes from phases other than anorthite and calcite. The emission peaks were spotted by SEM-CL, and fitted to 449.2(6) and 600(1) nm, respectively for anorthite and calcite. The two peaks appear together or not, depending on whether the analysed area contained or not calcite (Figure 4). A third emission, fainter at about 700 nm, was found but could not be related to a specific phase. No further fluorescence peaks were imaged.

The CL emission band around 450 nm was already observed in several plagioclase[13–15] and interpreted with the occurrence of Al—O^-—Al centres, in turn due to disordering in the tetrahedral cations. In anorthite, such disordering is kinetically inhibited, and the Al—O—Si-ordered configuration is thermodynamically stable up to the melting point.[16] However, some disorder, likely

defect induced, was observed in synthetic anorthite quenched close to the melting point.[17]

The emission at 600 nm is consistent with the presence of Mn^{2+} in calcite,[18,19] exchanging for Ca. A further emission, as well related to Mn^{2+}, but at 540 nm in plagioclase,[15] was not found here.

3.4 | Raman and fluorescence spectroscopies

Raman spectra are noisy due to the very high fluorescence. In the inclusion only anorthite, pyroxene and calcite are clearly identified by their principal peaks. In anorthite, we have the doublet of 485–505 cm^{-1}, related to the breathing modes of the four-membered tetrahedral rings,[20] in pyroxene the peak at 660 cm^{-1}, ascribed to the bending motion of the tetrahedral unique chain in monoclinic *C*2/*c* pyroxenes,[21] whereas in calcite, we observe the peak at 1085 cm^{-1} ascribed to the C—O symmetric stretching at 1085 cm^{-1}[[22]] (Figure 6). In anorthite, the difference in wavenumber between the peaks of the doublet was used to determine its composition according to Bersani et al.[23] determinative plot. The peak difference was measured in 15 spots, with an average difference of 16.4(1.5) cm^{-1}, which corresponds to a 95(4) % molar anorthite. Both Raman and SEM-EDS indicate that a slight but not negligible amount of Na is present in the anorthite.

Fluorescence was activated by the 473- and 632-nm laser. In both cases, a structured feature was observed at 690 nm (Figure 7). This feature was fitted via a Gaussian profile in three subpeaks at 678, 689 and 693 nm; it was in most cases, but not always, found together with the characteristic Raman peak doublet of anorthite at 485 and 505 cm^{-1}.

The peak position and structure, with the characteristic splitting and relative intensities of the split peaks, identify the emission as that of Cr^{3+} in octahedral configuration.[24] As Cr was present in microprobe analyses of anorthite, we could suggest that the emission is related to some small inclusion in anorthite, which would also

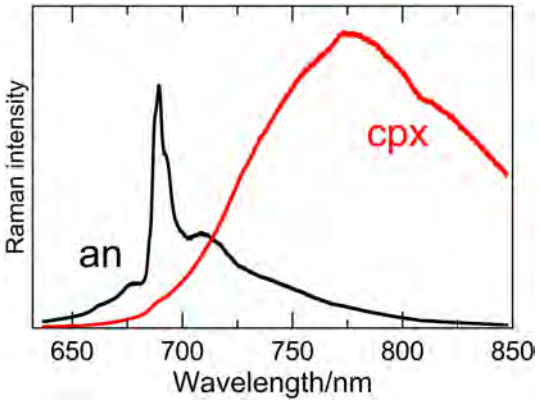

FIGURE 7 Major fluorescence peaks (632 nm emission): black, fluorescence from anorthite areas, likely due to Cr^{3+} in pyroxene, observed from red spots in the fluorescence map in Figure 8; red curve, fluorescence from the rim pyroxene, observed in green spots in Figure 8. The emission from calcite is like that of pyroxene, but with lower intensity. The corresponding range in wavenumber is 100–4000 cm^{-1} [Colour figure can be viewed at wileyonlinelibrary.com]

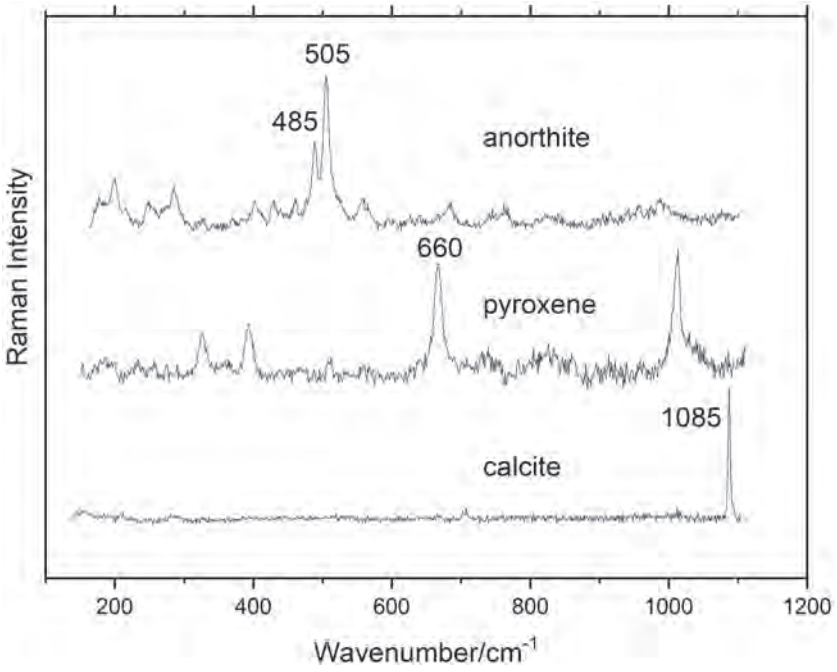

FIGURE 6 Raman spectra of phases in the Ca—Al inclusion and the position of the main peaks used for the mapping

account for the high Cr content. The octahedral configuration of Cr^{3+} does not fit with a substitution in plagioclase, as no octahedral site is present in plagioclase.[25] A possible candidate is Cr^{3+} in tiny inclusions, below SEM-EDS spatial resolution, of pyroxene in plagioclase, yet too small to be revealed by Raman observation: the observed spectrum is very similar to that of Cr^{3+} in the investigation on the optical properties of Cr^{3+} in the pyroxene spodumene[26]; moreover, the fluorescence spectra in the lower edge of the mapped image, where pyroxene is present in close contact with anorthite, shows the 690-nm peak, without coexisting anorthite Raman peaks. To note, SEM-EDS mapping could not reveal Cr-enriched areas. At higher wavelength, a broad peak, centred approximately at 720 nm, is present together with that of Cr (Figure 7). The position of the peak could correspond to that found as the red emission in feldspars, related to Fe^{3+} exchanging in the tetrahedral sites for Al,[15] and it is the same found in few CL spectra. The attribution is however uncertain, as Krbetschek et al.[27] showed that Fe emission in CL should occur in anorthite at lower wavenumber, at about 700 nm, as the position of the peak changes in plagioclase between 740 nm in albite and 700 nm in anorthite.

Fluorescence emissions of other phases are featureless, basically a large peak between 750 and 850 nm. The fluorescence emission in rim pyroxene was stronger than the others, providing the basis to map pyroxene (Figure 7).

3.5 | Combined mapping

A combined analysis of the maps obtained by SEM-EDS, CL and Raman peaks and fluorescence emissions was performed in the small area across the fassaitic pyroxene rim, where mapping of the Raman and the fluorescence was done. SEM-EDS Ca and Al maps show that the pyroxene is rimmed by a Na- and Cl-bearing phase, possibly sodalite. Anorthite is not in direct contact with the pyroxene rim, but with an interstitial Al and Ti richer pyroxene, displayed just at the bottom as a pink hue in Raman map in Figure 8. Anorthite secondary nature is revealed by patches of melilite within anorthite, indicating a likely absorption reaction (Figure 5). Moreover, the fluorescence emission map is defined by the two emissions, from the structured peak of Cr^{3+} at 690 nm and from the large band at 750–850 nm. The large band maps rim pyroxene and calcite together. The two emissions overlap the rim sodalite, not identified by Raman.

At a larger scale SEM-EDS, chemical maps together with optical CL show a complex intergrowth of different mineral phases. Following established patterns,[1] we find concentric rims, which conceal the primary texture. Spinel and melilite are only present as residual within an altered matrix. They are transformed in secondary fassaite and anorthite. It is not clear whether some fassaite is primary. A reaction rim of anorthite is present and could be sampled by CL analysis. Anorthite is a major phase within the inclusion, which conceals most of the original melilite. Anorthite is on its turn bordered with sodalite–nepheline, phases of alkaline alteration, after which secondary rim of fassaite is present. The sequence outlines most primary grains in the inclusion and is completed by final alteration via calcite formation.

3.6 | Comparison with other investigation on CAIs in CR2 chondrite

CAIs in CR carbonaceous chondrites were extensively studied. Makide et al.[28] in a comprehensive study showed that they are mostly of the spinel–melilite kind (118 over 166), and that in some case show grossular–perovskite–hibonite and ultrarefractory phases.[29] They are less abundant than in other carbonaceous chondrite families, like CV, about 1% of the volume,[30] and small, about 10–300 μm.[28] They are generally pristine: only few contain phyllosilicates, carbonates and sodalite; other phases are anorthite, and Al—Ti diopside. The CAI in this work Renazzo is off-trend for the larger size (1 × 2 mm), and for its significant, the alteration. The composition of the major phases, spinel, anorthite, melilite and diopside is close to those reported for the same minerals in previous investigations,[1,28] but with a significant alkaline imprinting. In melilite, we have a Na–akermanite component; in anorthite, we find several analyses with significant albite component, as shown also by the determination of the composition by Raman. The presence of sodalite, with a highly defective composition, and the finding of nepheline provide evidence for alkalization; moreover, alteration within the CAI is shown by phyllosilicates within the inclusion. We did not find reference to a detailed analysis of the texture in a CAI with such a pervasive alteration. In most studies, mineropetrographic features were approached as preliminary to oxygen or aluminium isotopic partitioning investigation,[28] looking for as much unaltered sample as possible.

In one of the few studies on metasomatism in carbonaceous chondrite, Brearley and Knot[31] showed a rather complex picture, with enrichment in hydrate phases, Fe rich like hedenbergite and alkali rich like sodalite and nepheline. Here, Fe-rich and hydrate phases are absent in the CAI, apart from a small rim, between anorthite and the rim pyroxene at the border of the inclusion (Figure 5).

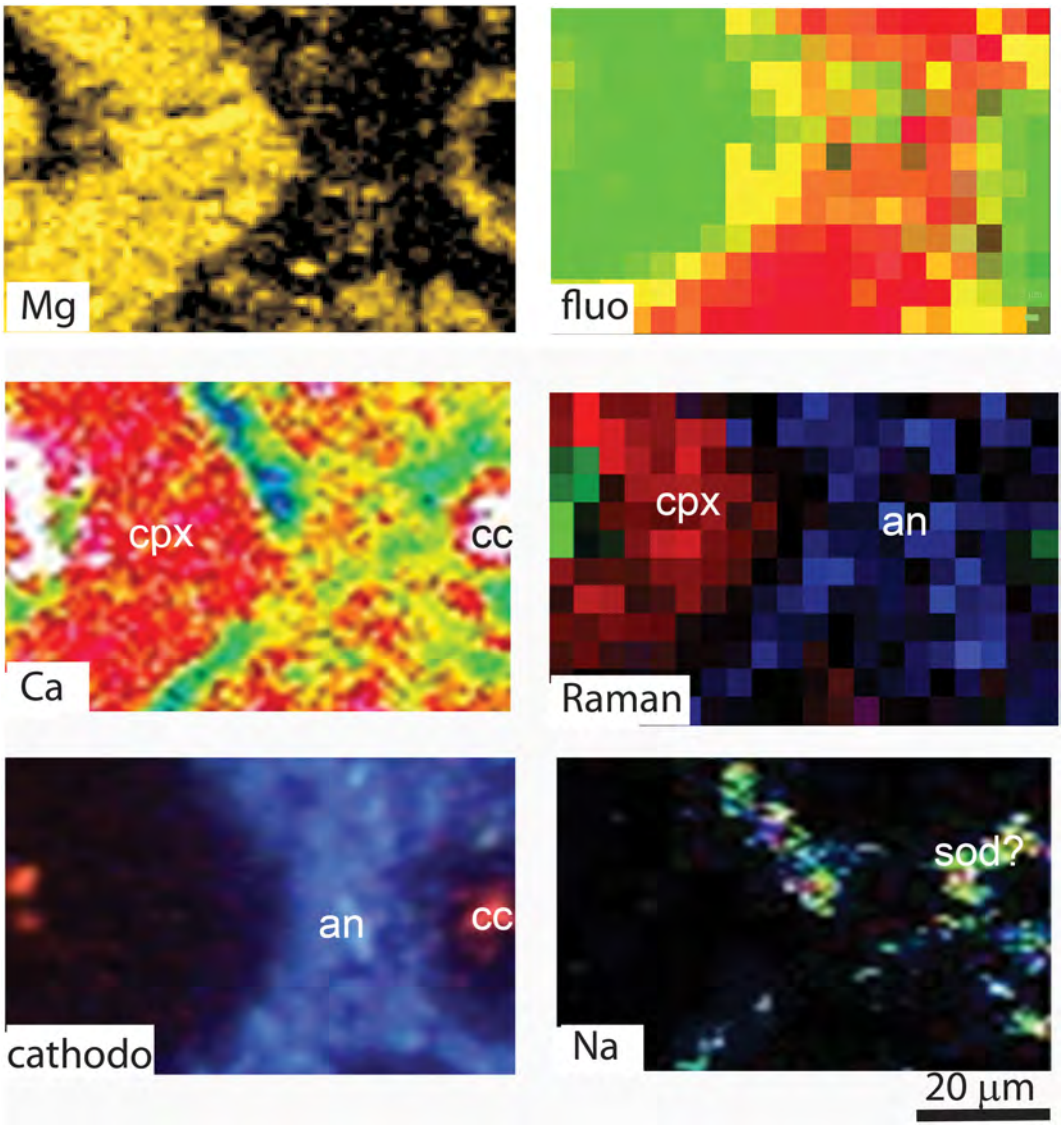

FIGURE 8 Comparative maps. Mg, Ca and Na, atomic distribution from scanning electron microscopy with energy dispersion system (SEM-EDS) chemical mapping, fluo: Raman fluorescence emissions: anorthite (an) and residual fassaite are mapped red, rim pyroxene (px) and calcite (cc) green, whereas intermediate fluorescence emission, likely related to alkali silicates is marked yellow; Raman, map from the peaks of anorthite (blue, 485 and 505 cm^{-1}), pyroxene (red, 660 cm^{-1}) and calcite (green, 1085 cm^{-1}); cathodo: cathodoluminescence from optical cathodoluminescence, blue anorthite, orange calcite [Colour figure can be viewed at wileyonlinelibrary.com]

4 | CONCLUSION

The CAI in the Renazzo CR2 chondrite formed as a fluffy type A inclusion, made by spinel and melilite, possibly with minor fassaite. In Figure 3, the optical CL shows that calcite and anorthite are never in contact and that calcite is present also within the matrix outside the inclusion, but not in the chondrules. Compositional EDS mapping, Raman and fluorescence maps show that sodalite and nepheline are in contact in the outer rim of anorthite and form a rim in external contact with calcite and pyroxene. Transformation in secondary anorthite has then occurred before an event of alkali alteration of Na- and Cl-bearing silicates. The alkali alteration is present only in the inclusion and thus predates the aggregation of the chondrite. The condensation of a few micrometres thick rim of secondary fassaite enveloped most of the grains and the whole inclusion. The picture is completed by an outer rim of calcite. Calcite is present also in the chondritic matrix, thus suggesting that it has occurred after the aggregation of the chondrite.

The above scenario was supported also by Raman spectroscopy; although only the main Raman peaks were visible, the fluorescence on itself may provide a map of the phases. We have observed that fluorescence and CL signals are complementary: using the different

wavelength of emission in laser can enhance signals that are overlapped by stronger ones in CL. The emission in anorthite, and in barely resolvable inclusions of pyroxene, observed in Raman-induced fluorescence at 690 nm, has strong similarities with Cr^{3+} emission from pyroxene. Such emission was not observed in pyroxene rim and could provide a difference between primary and secondary alteration fassaitic pyroxene. Further investigation in other inclusions should provide evidence for a possible pyroxene inclusion in secondary plagioclase and in the use of the 690-nm fluorescence peak as a reliable marker.

ACKNOWLEDGEMENTS

This work has benefited from the equipment and framework of the COMP-HUB Initiative, funded by the 'Departments of Excellednce' program of the Italian Ministry for Education, University and Research (MIUR, 2018–2022). Andrea Comelli is acknowledged for thin section preparation.

DATA AVAILABILITY STATEMENT

Data available on request from the authors.

ORCID

Mario Tribaudino https://orcid.org/0000-0003-4941-2914
Danilo Bersani https://orcid.org/0000-0002-8026-983X
Luciana Mantovani https://orcid.org/0000-0001-7438-1887
Giancarlo Salviati https://orcid.org/0000-0002-9828-6371

REFERENCES

[1] A. J. Brearley, R. H. Jones, *Planetary Materials*, Vol. 36, Mineralogical Society of America, Blacksburg (VA) **2019**.
[2] G. J. MacPherson, in *Treatise on Geochemistry* (Ed: A. M. Davis) Vol. 1, Elsevier, New York **2004**, pp. 201–246.
[3] J. N. Connelly, M. Bizzarro, A. N. Krot, Å. Nordlund, D. Wielandt, M. A. Ivanova, *Science* **2012**, *338*(6107), 651.
[4] Y. Amelin, A. N. Krot, I. D. Hutcheon, A. A. Ulyanov, *Science* **2002**, *297*, 1678.
[5] I. D. Hutcheon, I. M. Steele, J. V. Smith, R. N. Clayton, Proceedings of the 9th Lunar Science Conference **1978**, *9*, 1345.
[6] D. G. Akridge, J. M. C. Akridge, J. D. Batchelor, P. H. Benoit, J. Brewer, J. M. DeHart, B. D. Keck, L. Jie, A. Meier, M. Penrose, D. M. Schneider, D. W. G. Sears, S. J. K. Symes, Z. Yanhong, *J. Geophys. Res. E Planets* **2004**, *109*, 1.
[7] J. Garcia-Guinea, L. Tormo, O. Azumendi, J. Ruiz, V. Correcher, *Spectrosc. Lett.* **2011**, *44*, 516.
[8] M. M. Grady, G. Pratesi, V. Moggi, *Cecchi Atlas of Meteorites*, Cambridge University Press, Cambridge **2004**.
[9] M. K. Weisberg, M. Prinz, *Lunar Planet. Sci. Conf.* **1991**, *22*, 1483.
[10] M. K. Weisberg, M. Prinz, R. N. Clayton, T. K. Mayeda, *Geochim. Cosmochim. Acta* **1993**, *57*, 1567.
[11] D. A. Wark, J. F. Lovering, *Lunar Planet. Sci. Conf.* **1977**, *8*, 95.
[12] W. L. Brown, J. V. Smith, *Feldspar Minerals*, 2nd ed., Springer-Verlag, Berlin Heidelberg **1988**.
[13] Y. Kirsh, S. Shoval, P. D. Townsend, *Phys. Stat. Sol.* **1987**, *101*, 253.
[14] J. Götze, D. Habermann, U. Kempe, R. D. Neuser, D. K. Richter, *Am. Mineral.* **1999**, *84*, 1027.
[15] J. Götze, M. R. Krbetschek, D. Habermann, D. Wolf, in *Cathodoluminescence in Geosciences*, (Eds: M. Pagel, V. Barbin, P. Blanc, D. Ohnenstetter), Springer, Berlin, Heidelberg **2000** 245.
[16] M. A. Carpenter, *Phys. Chem. Miner.* **1992**, *19*, 1.
[17] P. Benna, G. Zanini, E. Bruno, *Contrib. Mineral. Petrol.* **1985**, *90*, 381.
[18] D. Habermann, R. D. Neuser, D. K. Richter, *Sediment. Geol.* **1998**, *116*, 13.
[19] M. Gaft, L. Nagli, G. Panczer, G. Waychunas, N. Porat, *Am. Mineral.* **2008**, *93*, 158.
[20] I. Aliatis, E. Lambruschi, L. Mantovani, D. Bersani, S. Andò, G. Diego Gatta, P. Gentile, E. Salvioli-Mariani, M. Prencipe, M. Tribaudino, P. P. Lottici, *J. Raman Spectrosc.* **2015**, *46*, 501.
[21] M. Prencipe, L. Mantovani, M. Tribaudino, D. Bersani, P. P. Lottici, *Eur. J. Mineral.* **2012**, *24*, 457.
[22] M. De La Pierre, C. Carteret, L. Maschio, E. André, R. Orlando, R. Dovesi, *J. Chem. Phys.* **2014**, *140*, 164509.
[23] D. Bersani, I. Aliatis, M. Tribaudino, L. Mantovani, A. Benisek, M. A. Carpenter, G. D. Gatta, P. P. Lottici, *J. Raman Spectrosc.* **2018**, *49*, 684.
[24] A. Finch, *Geol. Mag.* **2006**, *143*, 937.
[25] R. J. Angel, L. M. Sochalski-Kolbus, M. Tribaudino, *Am. Mineral.* **2012**, *97*, 765.
[26] E. O'Bannon, Q. Williams, *Am. Mineral.* **2016**, *101*, 1406.
[27] M. R. Krbetschek, J. Götze, G. Irmer, U. Rieser, T. Trautmann, *Mineral. Petrol.* **2002**, *76*, 167.
[28] K. Makide, K. Nagashima, A. N. Krot, G. R. Huss, I. D. Hutcheon, A. Bischoff, *Geochim. Cosmochim. Acta* **2009**, *73*, 5018.
[29] A. N. Krot, C. Ma, K. Nagashima, A. M. Davis, J. R. Beckett, S. B. Simon, M. Komatsu, T. J. Fagan, F. Brenker, M. A. Ivanova, A. Bischoff, *Geochemistry* **2019**, *79*, 125519.
[30] D. C. Hezel, S. S. Russell, A. J. Ross, A. T. Kearsley, *Meteorit. Planet. Sci.* **2008**, *43*, 1879.
[31] A. J. Brearley, A. N. Krot, in *Lecture Notes in Earth System Sciences*, (Eds: D. E. Harlov, H. Austrheim) Vol. 0, Springer Berlin Heidelberg, Berlin, Heidelberg **2013** 659.

SUPPORTING INFORMATION

Additional supporting information may be found in the online version of the article at the publisher's website.

How to cite this article: M. Tribaudino, D. Bersani, L. Mantovani, M. Pizzati, G. Salviati, *J Raman Spectrosc* **2021**, *52*(11), 1892. https://doi.org/10.1002/jrs.6234